# Atomic Clock Measurements of Quantum Scattering Phase Shifts Spanning Feshbach Resonances at Ultralow Fields

Aaron Bennett and Kurt Gibble*
*Department of Physics, The Pennsylvania State University, University Park, Pennsylvania 16802, USA*

Servaas Kokkelmans
*Eindhoven University of Technology, P.O. Box 513, 5600 MB Eindhoven, The Netherlands*

Jeremy M. Hutson†
*Joint Quantum Centre (JQC) Durham-Newcastle, Department of Chemistry, Durham University, South Road, Durham DH1 3LE, United Kingdom*

(Received 12 June 2017; published 15 September 2017)

We use an atomic fountain clock to measure quantum scattering phase shifts precisely through a series of narrow, low-field Feshbach resonances at average collision energies below 1 $\mu$K. Our low spread in collision energy yields phase variations of order $\pm\pi/2$ for target atoms in several $F$, $m_F$ states. We compare them to a theoretical model and establish the accuracy of the measurements and the theoretical uncertainties from the fitted potential. We find overall excellent agreement, with small statistically significant differences that remain unexplained.

DOI: 10.1103/PhysRevLett.119.113401

Coherence and the precise measurements allowed by long coherence times are central themes in atomic physics. The coherent nature of atom-atom scattering is important in phenomena such as Bose-Einstein condensation [1,2], Feshbach resonances [3–5], and ultracold molecule formation [6,7]. Atom-atom scattering also shifts the frequency of atomic clocks and interferometers [8–12], which often limits their precision and accuracy. Conversely, atom interferometry can directly probe the phase shifts at the core of quantum scattering [13–19] and sensitively test models of atom-atom interactions.

Accurate knowledge of low-energy scattering is especially important for cesium, as its clock collisional frequency shift is predicted to pass through zero around 100 nK [11]. This is the energy scale for collisions in PHARAO, a microgravity laser-cooled cesium clock scheduled to launch soon as part of the ACES mission [20]. Additionally, precise measurements of scattering phase shifts, or equivalently scattering lengths, near narrow Feshbach resonances may provide high sensitivity to the time variation of fundamental constants [21,22].

Here we use an atomic clock to make precision measurements of phase shifts for the scattering of ultracold cesium atoms through several narrow Feshbach resonances, as the magnetic field increases from 0 to 0.4 G. A narrow spread of collision energies allows us to observe phase-shift variations of nearly $\pi$ through the resonances. We establish the accuracy of our measurements and compare them to coupled-channel calculations that use recent interaction potentials from fits to Feshbach resonances and near-threshold bound states at fields from 10 to 1000 G [23]. We find overall excellent agreement with the model for the positions of the ultra-low-field Feshbach resonances, significantly improved from that obtained using the previous best interaction potential [5]. The absolute phase-shift differences also agree well, although some scattering channels show significant and yet-unexplained deviations.

Our interferometric technique [18,19] precisely and unambiguously detects differences of quantum scattering phase shifts [13–17]. Such information is difficult to extract from measurements of scattering cross sections, both because cold atom densities are challenging to measure accurately and because cross sections depend on the squares of scattering lengths. In our atomic fountain clock, a microwave $\pi/2$ pulse creates a coherent superposition of the cesium clock states $|F, m_F\rangle = |3, 0\rangle \equiv 3$ and $|4, 0\rangle \equiv 4$. The clock atoms then collide with "target" atoms in another state $|j\rangle \equiv |F, m_F\rangle$ with $s$-wave phase shifts $\delta_{3,j}$ and $\delta_{4,j}$, forming an outgoing spherical shell as shown in Fig. 1(a). Consequently, the phase of the scattered clock coherence, represented by the clock hands in Fig. 1(a), jumps by the difference of the $s$-wave phase shifts, $\Phi_j = \delta_{4,j} - \delta_{3,j}$. A second $\pi/2$ pulse with an adjustable phase yields a Ramsey fringe with the phase shift of the clock coherence $\Phi_j$. The scattered atoms are detected, and the atoms in the forward-scattering direction excluded, using a velocity-selective stimulated Raman transition [24]. This technique takes advantage of the phase and frequency accuracy of atomic clocks and precisely probes arbitrarily large phase differences. Several other techniques have also been demonstrated that precisely probe small differences of scattering lengths [2,25,26].

Scattering phase shifts change by $\pi$ as the magnetic field $B$ is scanned across a Feshbach resonance. However,

 

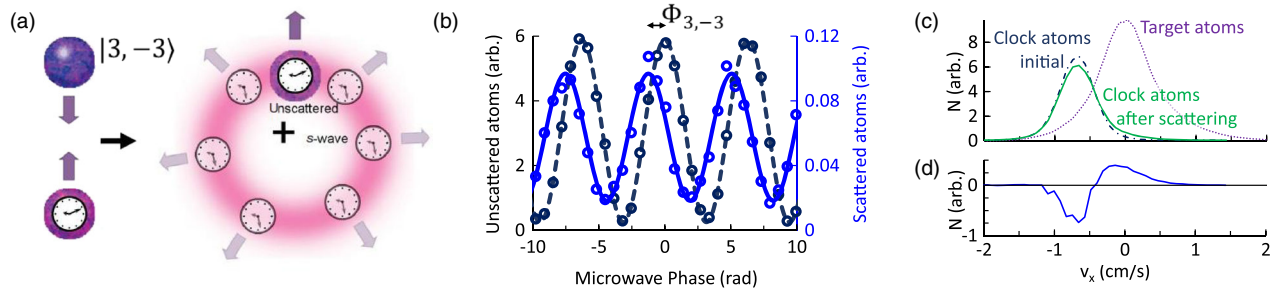


FIG. 1. (a) Atoms in a coherent superposition of the cesium clock states collide with atoms in a target state. The clock atom wave packet scatters as a spherically outgoing $s$-wave (pink shell) and continues unscattered (violet cloud). The clock faces indicate the differential scattering phase shift of the clock coherence. (b) Transition probability for scattered (solid blue) and unscattered (dashed grey) clock atoms. Each data point represents a single fountain launch with target atoms in $|3,-3\rangle$, a mean collision energy of $E_c = 798$ nK, and $B = 80$ mG. (c) After the first Ramsey pulse, the clock atoms prepared with dash-dot blue velocity distribution collide with the target atoms with the dotted purple distribution. The collisions redistribute the clock atom velocities (solid green). (d) Subtracting the initial clock velocity distribution from the distribution with scattering shows the net redistribution, which shifts the initial velocity class towards $v = 0$. The mean collision energy can be tuned by changing the initial selected and final detected velocity.

observing the full phase variation requires a narrow spread of collision energies. Our previous observations of cesium scattering phase shifts through Feshbach resonances studied the scattering between atoms in two distinct clouds [19] in our juggling atomic clock [13]. At collision energies $E_c$ between 12 and 50 $\mu$K, cloud temperatures even as low as 400 nK give a significant spread of collision energies, of order 10 $\mu$K, broadening the narrow resonances and suppressing the excursions of the phase shifts [19]. Here, we instead select and collide two velocity classes from a single launched cloud in our fountain clock. The low collision energies of 0.5 to 1 $\mu$K and correspondingly narrow energy spread yield observed phase-shift variations of nearly $\pi$ through several narrow Feshbach resonances.

Our experimental sequence begins with launching atoms from a magneto-optical trap and cooling them to 400 nK with degenerate sideband cooling in a moving-frame 3D optical lattice [18,19,27]. After the sideband lattice cooling, 65% of the atoms are in $|3,3\rangle$, 20% are in $|3,2\rangle$, and the rest are in other $|3,m_F\rangle$ states. The atoms in $|3,3\rangle$ are transferred to the desired target state, $|3,m_F = \pm 1,\pm 2,\pm 3\rangle$ or $|4,m_F \neq 0\rangle$, by a series of microwave pulses. To prepare $m_F < 0$ target states, a nonadiabatic magnetic field reversal precedes the microwave pulses to transfer the atoms from $|3,3\rangle$ to $|3,-3\rangle$. For all targets except $|3,\pm 1\rangle$ [28,29], the atoms initially in $|3,2\rangle$ are transferred to either $|3,0\rangle$ or $|4,0\rangle$ by another series of microwave pulses, interleaved with the target-atom microwave pulses, and a stimulated Raman pulse. The Raman pulse is velocity sensitive and selects a slice of the velocity distribution, 36 nK wide, in the horizontal $x$ direction, imparting two photon recoils to the selected atoms, as in Fig. 1(c). Unwanted atoms in other $m_F < 0$ states and other velocity classes are removed with clearing laser pulses tuned to the $6S_{1/2} \rightarrow 6P_{3/2}$, $F = 3 \rightarrow 5'$ and $3 \rightarrow 2'$ transitions. A $\pi/2$ microwave pulse then prepares the clock atoms in a coherent superposition of $|3,0\rangle$ and $|4,0\rangle$, after which the collisions of the clock atoms with the target atoms above the clock cavity change their velocities $v$. In Fig. 1(c), the collisions tend to scatter atoms with large velocities towards $v = 0$ [30] as they begin to thermalize. For the small fraction of clock atoms that scatter, the phase of the clock coherence is shifted by the difference of the $s$-wave scattering phase shifts [18]. After the atoms fall back into the cavity, a second microwave $\pi/2$ pulse produces the Ramsey fringe in Fig. 1(b). A clearing pulse removes the target atoms, as well as the clock atom population in the same hyperfine state $F$ as the target atoms. For $|4,m_F\rangle$ target atoms, a stimulated Raman transition (the Raman probe) transfers a narrow velocity class of scattered atoms, 36 nK wide, to $|4,0\rangle$. A laser resonant with the $4 \rightarrow 5'$ transition excites these atoms and we collect their fluorescence to obtain Fig. 1(b). In Fig. 1(b), we also measure a reference Ramsey fringe, where we clear the target atoms before the first Ramsey pulse and detect atoms at the center of the clock-atom velocity distribution. For $|3,m_F\rangle$ target atoms, an additional microwave pulse after the $F = 3$ clearing pulse transfers the clock atoms in $|4,0\rangle$ to $|3,0\rangle$, and then a second clearing pulse removes $F = 4$ atoms before a stimulated Raman probe as above. We evaluate and subtract backgrounds using a pump-probe technique that clears the target atoms immediately before the first Ramsey pulse, inhibits the clock-atom Raman selection, or both, to yield the Ramsey fringes as shown in Fig. 1(b) [18,19,30].

Figure 2 shows the measured phase shifts for target atoms in each $|F,m_F \neq 0\rangle$ state, as we traverse a number of low-field Feshbach resonances. Each panel shows the measured phase shifts for mean collision energies of 656 and 798 nK [31], which is changed by selecting a different detected velocity of the scattered clock atoms. Results for target atoms with positive or negative $m_F$ are shown at magnetic fields with opposite signs, producing plots that

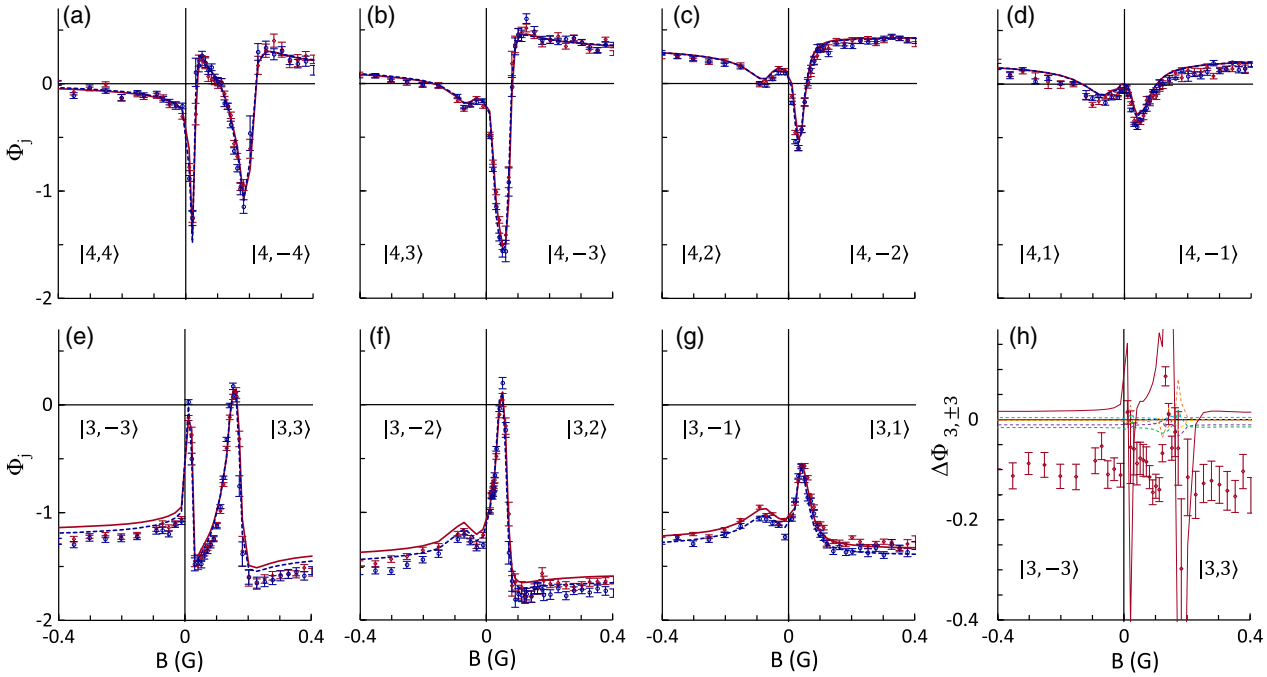


FIG. 2. (a)–(g) Magnetic field dependence of the differential phase shift $\Phi_j$ for target atoms in the $|4, m_F \neq 0\rangle$ and $|3, m_F \neq 0\rangle$ states; negative $B$ corresponds to the opposite sign of $m_F$. The scattering phase shifts vary rapidly with magnetic field through a series of Feshbach resonances. The blue circles (red diamonds) are experimental results for mean collision energies of 616–656 nK (746–798 nK) and the curves are corresponding energy-averaged results from coupled-channel calculations on the best-fit potential [23]. (h) Comparison of measured (red diamonds) and theoretical values of $\Phi_{3,\pm3}$. All are shown after subtracting $\Phi_{3,\pm3}$ from the best-fit potential [23]. The best-fit potential and experimental results differ by ≈0.1 rad throughout the range and their variations through the Feshbach resonances agree very well. The previous best potential (solid red line) [5] gives much larger deviations from experiment through the resonances. The six dashed curves indicate the uncertainty of the best-fit potential. Their differences from the best-fit potential are small compared to the ≈0.1 rad offset of the experimental results.

are continuous through $B = 0$. The Feshbach resonances for 656 nK occur at lower magnetic fields than those for 798 nK, and we observe slightly larger phase variations through the resonances, as expected from the smaller spread of collision energies. The error bars are the quadrature sum of the statistical and systematic uncertainties, typically 30 mrad for 10 min of averaging at points far from resonances. Through the resonances, where the scattering cross section passes through zero, they may be as large as 100 mrad after 20 min of averaging.

There are distinct similarities between the resonance positions and profiles for target atoms $|3, \pm|m_F|\rangle$ and $|4, \mp(|m_F| + 1)\rangle$. In Figs. 2(a)–2(g), we observe two clear resonant features. For target atoms in $|3, 3\rangle$ and $|4, -4\rangle$, these resonances are near 20 and 180 mG. For each of the other target states, one resonance is near 50 mG and the other near −80 mG. We do not expect any resonances for target atoms in $|3, -3\rangle$ and $|4, 4\rangle$ because conservation of angular momentum prohibits coupling to any closed $s$-wave channels with halo states. While we observe only two resonant features for each $|m_F|$, there are additional resonances that are not resolved, because they overlap or are too narrow. For example, the results in Ref. [19] indicate that there are two Feshbach resonances for $|3, 2\rangle$ target atoms, while here we see only one. We show experimentally that these resonances are in scattering channels with clock and target atoms in different hyperfine levels, e.g., $|4, 0\rangle$ and $|3, 3\rangle$, by measuring velocity-changing cross sections [30].

The amplitude of the phase variation is different for each resonant feature. We observe variations of nearly $\pi$ for some resonances, but others produce variations as small as a few hundred mrad. The scattering phase shift wraps through $\pi$ across an elastic Feshbach resonance, but even in the elastic limit we will observe a smaller variation if the resonance is narrower than our spread of collision energies. Inelastic loss may also reduce the amplitude of the phase variations. Additional sharp phase changes may be caused by the closing of inelastic scattering channels, but these are usually smaller and do not wrap through $\pi$.

Figure 2 also shows the results of coupled-channel calculations performed with the MOLSCAT quantum scattering package [32], using the interaction potentials of Berninger *et al.* [23]. The experimental observable is the Ramsey fringe in Fig. 1(b), which results from the interference of the scattered atoms only, given by a quantity $J = \langle |f_{3,j} + f_{4,j}|^2 \rangle$ [33]. Here the brackets denote an energy average, and $f_{3,j}$ and $f_{4,j}$ indicate the scattering

amplitudes for atoms in states 3 and 4, respectively, colliding with an atom in state $j$. The phase of the fringe is shifted by the effect of the collisions, and is directly related to the interference term in $J$. The phase shift can therefore be expressed as $\Phi_j = \arg\langle T_{3,j} T^*_{4,j}\rangle$, where $T_{3,j}$ and $T_{4,j}$ are the diagonal $T$-matrix elements corresponding to the scattering amplitudes $f_{3,j}$ and $f_{4,j}$.

The $T$-matrix elements may be written exactly in terms of complex $k$-dependent scattering lengths $a$, $T = 2ika/(1+ika)$ [34]. This gives

$$\Phi_j = \arg\left\langle \left(\frac{2ika_{3,j}}{1+ika_{3,j}}\right)\left(\frac{-2ika^*_{4,j}}{1-ika^*_{4,j}}\right)\right\rangle. \quad (1)$$

Writing $a = \alpha - i\beta$, $1 + ika = 1 + k\beta + ik\alpha$ has a phase $\arctan[k\alpha/(1+k\beta)]$. If the range of energies is narrow, Eq. (1) reduces to

$$\Phi_j \approx -\arctan\left(\frac{k\alpha_{3,j}}{1+k\beta_{3,j}}\right) + \arctan\left(\frac{k\alpha_{4,j}}{1+k\beta_{4,j}}\right) + \arg(a_{3,j}) - \arg(a_{4,j}). \quad (2)$$

When the scattering is purely elastic, $a$ is real, and Eq. (2) reduces to the difference between the scattering phase shifts $\Phi_j = \delta_{4,j} - \delta_{3,j}$, with $\delta = -\arctan ka$. At zero collision energy, $\delta_{4,j} - \delta_{3,j}$ vanishes, but, in the presence of inelasticity, the phases $\arg(a)$ contribute to $\Phi_j$ and persist to zero energy. Note that our coupled-channel calculations evaluate the full expression (1) for $\Phi_j$, including inelastic contributions.

The coupled-channel calculations are in overall excellent agreement with the experimental results. The resonance positions and profiles are well reproduced. Away from the Feshbach resonances, the background phase-shift differences $\Phi_{4,m_F}$ depend weakly on collision energy and agree quite well with the theoretical model. However, those for $|3, m_F\rangle$ target atoms show significant energy dependences and small but statistically significant differences with the theoretical model.

To estimate the uncertainty in the predictions of the fitted potential, we have repeated the fits of Ref. [23] and determined uncorrelated directions in the six-parameter space. We have then found a potential shifted in each of these directions by an amount that doubles the sum of squares of residuals $\chi^2$ for the original data set of Ref. [23]. For a locally linear fit, these correspond to approximately $5\sigma$ uncertainties. We have repeated the coupled-channel calculations of $\Phi_j$ for these six potentials. The differences from the best-fit potential are small, and are shown for $|3, \pm 3\rangle$ in Fig. 2(h), together with corresponding differences for the experimental results. For other targets, the differences between the shifted potentials and the best-fit potential are even smaller. We conclude that the remaining differences between experiment and theory are well outside the range of the uncertainties from the interaction potential derived from the experiments of Ref. [23].

Figure 2(h) also shows the results obtained from coupled-channel calculations using the previous best potential [5], also plotted as differences from the best-fit potential. For $|3, \pm 3\rangle$ and the other target states, the potential from [23] gives substantially better agreement through the resonances. The details of the bound states that cause the low-field resonances are beyond the scope of this Letter. In essence, however, there is a group of pure triplet states bound by only 3.7 kHz at zero field that, as a function of magnetic field, are far from parallel to the atomic thresholds below 0.1 G. Their crossings with the thresholds cause the resonances we observe. At higher fields they mix with more deeply bound states that possess some singlet character, and eventually become almost parallel to the atomic thresholds at fields above 0.3 G.

To achieve the accuracy of these measurements, the experimental sequence above avoids and accounts for several systematic errors. The largest remaining systematic correction applied to the results in Fig. 2 comes from the interference between the scattered and unscattered waves. This gives the usual loss of atom current in the forward-scattering direction, producing the dip in the distribution in Fig. 1(d) and contributing a different phase to the scattered Ramsey fringe in Fig. 1(b). We determine this contribution as a function of the probed velocity: the phase shift of the interference current is approximately zero and, therefore, when $\Phi_j$ is far from 0, the correction can be significant [28]. For the background $\Phi_{3,m_F=(1,2,3)}$, this correction is about (80,80,120) mrad for our low energy and (40,70,100) mrad for our high energy, increasing $\Phi_{3,m_F}$ (closer to the theory) with a typical uncertainty of 25 mrad. The differences in Fig. 2(h) for $|3, \pm 3\rangle$ are significantly larger than this systematic uncertainty. Another significant systematic arises because the scattered atoms experience a cold-collision frequency shift from the target atoms [8,12], in addition to the differential scattering phase shift. Our sequence evaluates and corrects for this collision shift by measuring the collision shift of the unscattered atoms (forward direction) due to the target atoms [28,29]. The correction is typically $-40(0) \pm 3$ mrad for $\Phi_{3(4),m_F}$. We also apply a small correction due to inelastic spin-changing collisions populating other $|F, m_F\rangle$ target states [28,29].

In summary, we precisely measure quantum scattering phase shifts spanning a series of Feshbach resonances and compare them to a state-of-the-art theoretical model. These results provide a stringent confirmation of the cesium interaction potentials of Ref. [23], but small, statistically significant, differences remain unexplained. We have considered the uncertainties in the theoretical predictions due to statistical uncertainties in the fitted interaction potentials and shown them to be very small. The theory shows that inelastic processes make important contributions to the

observable quantities that persist even in the limit of zero collision energy. With this experimental technique, we can currently determine differential scattering phase shifts with mrad precision in less than a day of averaging. Further work using these and further improved interaction potentials may probe how this technique can best set stringent limits on the time variation of fundamental constants, such as the electron-proton mass ratio, by observing the constancy of the scattering phase shifts near narrow Feshbach resonances [21,22].

We are grateful to S. Gensemer for contributions during the initial stages of this experiment, to C. R. Le Sueur for work to modify MOLSCAT to handle asymptotically degenerate states, and to E. Tiesinga for stimulating discussions. We acknowledge financial support from the National Science Foundation, National Aeronautics and Space Administration, The Pennsylvania State University, and the UK Engineering and Physical Sciences Research Council under Grants No. EP/I012044/1, No. EP/N007085/1, and No. EP/P01058X/1. This work is part of the Vici research programme with Project No. 680-47-623, which is financed by the Netherlands Organisation for Scientific Research (NWO).

*kgibble@psu.edu
†J.M.Hutson@durham.ac.uk

[1] D. S. Hall, M. R. Matthews, J. R. Wieman, C. E. Wieman, and E. A. Cornell, Phys. Rev. Lett. **81**, 1539 (1998).
[2] A. Widera, F. Berbier, S. Folling, T. Gericke, O. Mandel, and I. Bloch, New J. Phys. **8**, 152 (2006).
[3] C. Chin, R. Grimm, P. Julienne, and E. Tiesinga, Rev. Mod. Phys. **82**, 1225 (2010).
[4] S. Inouye, M. R. Andrews, J. Stenger, H. J. Miesner, D. M. Stamper-Kurn, and W. Ketterle, Nature (London) **392**, 151 (1998).
[5] C. Chin, V. Vuletic, A. J. Kerman, S. Chu, E. Tiesinga, P. J. Leo, and C. J. Williams, Phys. Rev. A **70**, 032701 (2004).
[6] C. A. Regal, C. Ticknor, J. L. Bohn, and D. S. Jin, Nature (London) **424**, 47 (2003).
[7] J. Herbig, T. Kraemer, M. Mark, T. Weber, C. Chin, H. C. Nägerl, and R. Grimm, Science **301**, 1510 (2003).
[8] K. Gibble and S. Chu, Phys. Rev. Lett. **70**, 1771 (1993).
[9] C. Fertig and K. Gibble, Phys. Rev. Lett. **85**, 1622 (2000).
[10] F. P. Dos Santos, H. Marion, S. Bize, Y. Sortais, A. Clairon, and C. Salomon, Phys. Rev. Lett. **89**, 233004 (2002).
[11] K. Szymaniec, W. Chalupczak, E. Tiesinga, C. J. Williams, S. Weyers, and R. Wynands, Phys. Rev. Lett. **98**, 153002 (2007).
[12] D. J. Papoular, S. Bize, A. Clairon, H. Marion, S. J. J. M. F. Kokkelmans, and G. V. Shlyapnikov, Phys. Rev. A **86**, 040701(R) (2012).
[13] R. Legere and K. Gibble, Phys. Rev. Lett. **81**, 5780 (1998).
[14] N. R. Thomas, N. Kjærgaard, P. S. Julienne, and A. C. Wilson, Phys. Rev. Lett. **93**, 173201 (2004).
[15] C. Buggle, J. Léonard, W. von Klitzing, and J. T. M. Walraven, Phys. Rev. Lett. **93**, 173202 (2004).
[16] T. Volz, S. Dürr, N. Syassen, G. Rempe, E. van Kempen, and S. Kokkelmans, Phys. Rev. A **72**, 010704 (2005).
[17] A. S. Mellish, N. Kjærgaard, P. S. Julienne, and A. C. Wilson, Phys. Rev. A **75**, 020701 (2007).
[18] R. A. Hart, X. Xu, R. Legere, and K. Gibble, Nature (London) **446**, 892 (2007).
[19] S. D. Gensemer, R. B. Martin-Wells, A. W. Bennett, and K. Gibble, Phys. Rev. Lett. **109**, 263201 (2012).
[20] P. Laurent *et al.*, Appl. Phys. B **84**, 683 (2006).
[21] C. Chin and V. V. Flambaum, Phys. Rev. Lett. **96**, 230801 (2006).
[22] A. Borschevsky, K. Beloy, V. V. Flambaum, and P. Schwerdtfeger, Phys. Rev. A **83**, 052706 (2011).
[23] M. Berninger, A. Zenesini, B. Huang, W. Harm, H.-C. Nägerl, F. Ferlaino, R. Grimm, P. S. Julienne, and J. M. Hutson, Phys. Rev. A **87**, 032517 (2013).
[24] M. Kasevich, D. S. Weiss, E. Riis, K. Moler, S. Kasapi, and S. Chu, Phys. Rev. Lett. **66**, 2297 (1991).
[25] M. R. Matthews, D. S. Hall, D. S. Jin, J. R. Ensher, C. E. Wieman, E. A. Cornell, F. Dalfovo, C. Minniti, and S. Stringari, Phys. Rev. Lett. **81**, 243 (1998).
[26] M. Egorov, B. Opanchuk, P. Drummond, B. V. Hall, P. Hannaford, and A. I. Sidorov, Phys. Rev. A **87**, 053614 (2013).
[27] P. Treutlein, K. Y. Chung, and S. Chu, Phys. Rev. A **63**, 051401 (2001).
[28] A. Bennett, Ph.D. thesis, Pennsylvania State University, 2015.
[29] See Supplemental Material at http://link.aps.org/supplemental/10.1103/PhysRevLett.119.113401 for experimental details.
[30] K. Gibble, S. Chang, and R. Legere, Phys. Rev. Lett. **75**, 2666 (1995).
[31] These mean collision energies are weighted by $E_c^{-1}$ to account for the energy dependence of $(\pi^2/k^2)T_3T_4^*$ near 1 $\mu$K. For $|3(4),\pm1\rangle$, the selection width is 13 nK and the mean energies are 644(616) and 771(746) nK. The spread of collision energies for low and high energy are 428 and 461 nK for $m_F \neq \pm 1$ and 416(407) and 437(434) nK for $|3(4),\pm1\rangle$.
[32] J. M. Hutson and S. Green, computer program MOLSCAT, version 14, UK Engineering and Physical Sciences Research Council, 1994.
[33] S. J. J. M. F. Kokkelmans, Ph.D. thesis, Technische Universiteit Eindhoven, 2000.
[34] J. M. Hutson, New J. Phys. **9**, 152 (2007).

# Supplemental Material

## EXPERIMENTAL APPARATUS

Our cesium atomic clock is depicted in Fig. S1. It has previously been described in [18, 19]. Atoms are collected in the vapor cell magneto-optical trap (MOT) and multiply launched into the ultra-high vacuum (UHV) MOT. They are then launched and loaded into a moving-frame optical lattice to optically pump and cool the atoms to 400 nK. State preparation cavities (SPC) resonant at 9.2 GHz drive microwave transitions to prepare the atoms in specific $|F, m_F\rangle$ states. The Raman beams counter-propagate and select the clock atoms as they travel upwards, followed by probing the atoms as they return from the clock cavity. The clearing beams push atoms in the $F = 3$ or $F = 4$ hyperfine states to remove them from their fountain trajectory. In this experiment, the tube cavity serves as the clock cavity, exciting the atoms at its lowest field antinode. This fountain has no magnetic shielding for static magnetic fields. A long aluminum cylinder, with a wall thickness of 0.5 inches, surrounds SPC 4 and the tube cavity, to shield a small ambient 60 Hz magnetic field and its higher harmonics.

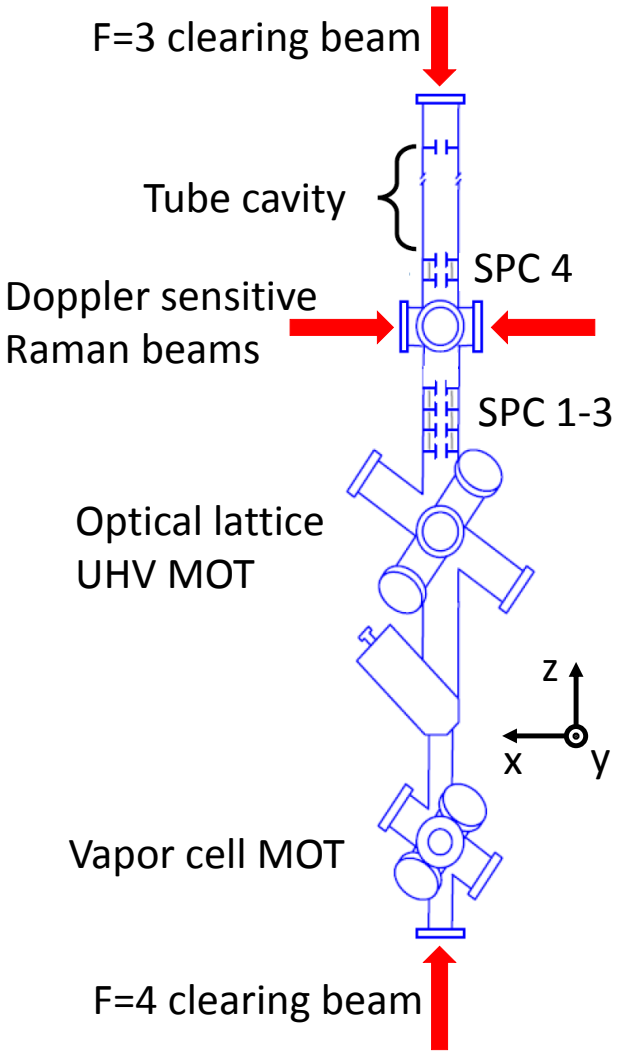


FIG. S1. (color online). Cesium atomic fountain clock schematic.

## EXPERIMENTAL SEQUENCE FOR $|3, \pm 1\rangle$ TARGETS

For $|3, \pm 1\rangle$ targets, our sequence draws the target and clock atoms from $|3, 3\rangle$. Microwave pulses first transfer atoms launched in $|3, 3\rangle$ to $|4, 0\rangle$, followed by a Raman selection that transfers a portion of the atoms to $|3, \mp 1\rangle$. A microwave pulse then transfers the unselected atoms in $|4, 0\rangle$ to $|3, \pm 1\rangle$. We then clear F=4 and transfer the selected atoms back to $|4, 0\rangle$. With the target atoms in $|3, \pm 1\rangle$ and the clock atoms in $|4, 0\rangle$, the sequence follows that for other $|3, m_F\rangle$ targets.

## SYSTEMATIC ERRORS

### Frequency Shift due to Ultracold Collisions

We ascertain the cold collision shift using additional experimental sequences to measure the Ramsey fringes of the unscattered atoms with target atoms present and with the target atoms cleared just before the first Ramsey pulse. However, because the scattered and unscattered atoms have slightly different fountain trajectories, this measured correction is not exact. We therefore also measure $\Phi$ as a function of target atom density and extrapolate the measured phase shifts to zero density to confirm independently that the error of this correction is safely less than the statistical error bars [28]. Because these collision shifts result from an interference between the scattered and incident atom waves, their values depend on the scattering phase shifts and we therefore observe significant variations of the collision shifts through Feshbach resonances. Ref. [12] reported related measurements of the ratios of the frequency shift for clock state and $F = 3$ target atoms between $-80$ and 100 mG.

### Corrections due to Inelastic Collisions

We also correct our measurements of $\Phi$ for a systematic error due to inelastic spin-changing collisions that populate other $|F, m_F\rangle$ target states. For example, inelastic collisions between target atoms in $|3, 2\rangle$ populate $|3, 1\rangle$ and $|3, 3\rangle$ (see Fig. S2). Inelastic collisions that conserve $F$ produce a systematic error because $\Phi_{3,1}$ and $\Phi_{3,3}$ are different from $\Phi_{3,2}$. Our sequence minimizes this

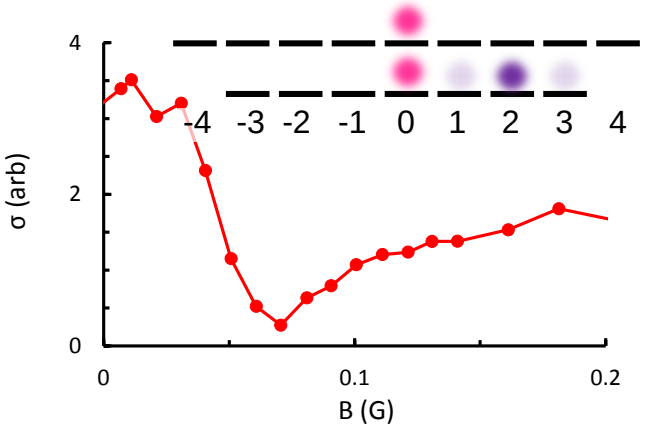


FIG. S2. (color online). Inelastic collisions between target atoms in $|3,2\rangle$ populate the $|3,1\rangle$ and $|3,3\rangle$ states. When the scattering cross section for collisions between the intended clock and target state goes to zero, the fractional contribution to the scattered Ramsey fringes from clock atoms colliding with the inelastically populated states can be significant.

error by transferring the target atoms to the target state just before the first Ramsey pulse and clears atoms that scattered inelastically up to that point in the fountain trajectory. Because the number of inelastic collisions is small, this error is only significant when the scattering cross section of the intended target and clock states approaches zero through a Feshbach resonance, as shown in Fig. S2 for $|3,2\rangle$ target atoms. Similar inelastic collisions occur between clock and target atoms, but because the clock atom density is $\approx 20$ times smaller than the target cloud density, populations in unintended states from inelastic collisions involving clock atoms are negligible. Between 50 and 100 mG, clock atoms colliding with $|3,1\rangle$ and $|3,3\rangle$ contribute significantly to the phase of the scattered Ramsey fringe. The results in Fig. 2 include this correction, as large as 75 mrad and comparable to the statistical error bars of about 100 mrad [28].

### Magnetic field stability and uniformity

To reduce background fluctuations in the magnetic field, we actively stabilize all three components of the vector field using a flux gate magnetometer and a digital servo. The residual field noise is $\pm 50$ $\mu$G, which produces noise due to the quadratic Zeeman shift at a bias field of 0.4 G that is below our background noise. We also minimize gradients of the magnetic field in the flight region, which can give a systematic error since the atoms that produce the scattered and unscattered Ramsey fringes in Fig. 1b follow different trajectories and therefore experience different quadratic Zeeman shifts. The field is in the vertical ($z$) direction so we minimize the gradients $\frac{dB_z}{dz}$, $\frac{dB_z}{dy}$, and $\frac{dB_z}{dx}$. To reduce $\frac{dB_z}{dz}$, we measure the $|3,3\rangle$ to $|4,3\rangle$ transition frequency at various heights above the clock cavity and apply correction currents to coils surrounding the apparatus. To measure and null $\frac{dB_z}{dy}$, we drive the same magnetically sensitive transition but mask opposite halves of the detection beam on successive shots, probing the field in either the positive or negative $y$ half of the fountain. To measure and minimize $\frac{dB_z}{dx}$, we use photon recoils from a pair of Raman beams to push the cloud in opposite directions before driving the magnetically sensitive transition. We then adjust the field so that the atoms experience the same magnetic field whether they are pushed in the positive or negative $x$ direction. We subsequently observe Ramsey fringes for recoils in opposite directions with phase differences less than 10 mrad at 400 mG [28].